

FE-LWS: Refined Image-Text Representations via Decoder Stacking and Fused Encodings for Remote Sensing Image Captioning

Swadhin Das, *Graduate Student Member, IEEE*, Raksha Sharma, *Member, IEEE*

Abstract—Remote sensing image captioning (RSIC) aims to generate meaningful textual descriptions from remote sensing images using encoder-decoder frameworks. Although previous efforts have focused primarily on improving the design of decoders, significant challenges persist in capturing the complex spatial and semantic characteristics of remote sensing data. In addition, reliance on a single encoder or decoder often limits the representational capacity of the model. To address these limitations, we propose a novel framework that fuses features from two complementary CNN encoders and integrates a stacked GRU decoder with weighted averaging to better model multilevel semantics. Experimental evaluations demonstrate that the proposed approach outperforms existing baselines, delivering more accurate and contextually rich captions for remote sensing images.

Index Terms—Remote Sensing Image Captioning (RSIC), Encoder-Decoder model, Convolutional Neural Network (CNN), Gated Recurrent Unit (GRU), Fusion-based Encoders (FE), Weighted-based Stacking (WS).

I. INTRODUCTION

Remote Sensing Image Captioning (RSIC) is a task in the machine learning domain that focuses on extracting meaningful information from a remote sensing images. The encoder-decoder framework is the dominant approach in RSIC, where a CNN-based encoder (such as ResNet [1], ConvNext [2]) extracts image features and a decoder (e.g., LSTM [3], [4], GRU [5], or SVM [6]) generates captions in sequence-to-sequence manner.

Although decoder optimization has received considerable attention [3], [7], the encoder's role in capturing spatial and semantic diversity remains underexplored. Most of the methods are based on a single CNN, which limits the representational richness. To address this, we propose a fusion-based encoder that integrates features from two complementary CNNs, enabling a more detailed and robust image understanding.

Similarly, most existing models employ a single decoder, which restricts the modeling of hierarchical semantics and long-range dependencies [4], [8], [9]. We adopt a stacked GRU-based decoder [10], [11] to sequentially refine features across layers, improve contextual representation, and

mitigate vanishing gradients. To avoid losing intermediate information, we aggregated the outputs of all decoder layers using a weighted averaging strategy, allowing the model to capture both low and high-level semantics more effectively.

The major contributions of this letter are as follows.

- A fusion-based encoding strategy is proposed to enhance image representation and understanding.
- A novel multi-layer stacked GRU decoder with weighted averaging is proposed to improve sequence modeling.
- The proposed model is thoroughly evaluated against state-of-the-art methods, demonstrating its notable performance improvement.

The structure of the letter is as follows: Section II introduces our proposed approach, focusing on fusion-based encoding and stacking-based decoding techniques. Section III describes the experimental setup, covering datasets, model configurations, and evaluation metrics. Section IV presents the results of various aspects, including ablation studies of our model, and provides a comparative analysis with baseline models through both quantitative and qualitative evaluations, supported by visual examples. Finally, Section V summarizes the key findings of the letter and highlights potential avenues for future research.

II. PROPOSED METHOD

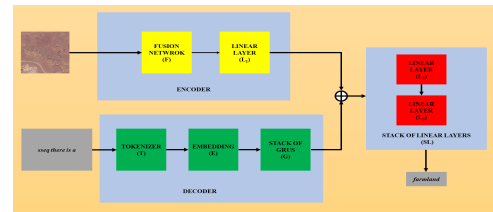


Fig. 1: Architecture of the Proposed Model

The overall architecture is illustrated in Figure 1. We adopt an encoder-decoder framework, where the encoder (F) consists of two distinct CNNs whose outputs are concatenated and processed through a linear transformation layer (L_1). For decoding, a tokenized input sequence passes through an embedding layer (E) and then into a stack of Gated Recurrent Units (GRU) (G) to model

Manuscript received July 2025

Both the authors are from Department of Computer Science and Engineering, Indian Institute of Technology, Roorkee, India (e-mails are: {s_das,raksha.sharma}@cs.iitr.ac.in).

TABLE I: Performance Comparison of Individual and Fusion-Based CNN Encoders on the SYDNEY Dataset

CNN	BLEU-1	BLEU-2	BLEU-3	BLEU-4	METEOR	ROUGE-L	CIDEr
ConvNext	0.7531	0.6645	0.5982	0.5376	0.3750	0.6951	2.3954
ResNet	0.7363	0.6502	0.5785	0.5138	0.3621	0.6809	2.2526
ResNet	0.7415	0.6556	0.5845	0.5209	0.3625	0.6706	2.2912
DenseNet	0.7214	0.6333	0.5621	0.4935	0.3419	0.6314	2.1444
ConvNext-ResNet	0.7679	0.6814	0.6084	0.5458	0.3801	0.7263	2.4515
ConvNext-ResNet	0.7582	0.6727	0.6039	0.5438	0.3808	0.7164	2.3882
ConvNext-DenseNet	0.7419	0.6571	0.5823	0.5264	0.3822	0.6911	2.3755
ResNet-ResNet	0.7517	0.6664	0.5924	0.5243	0.3789	0.6963	2.3515
ResNet-DenseNet	0.7246	0.6413	0.5722	0.5101	0.3644	0.6798	2.2488
ResNext-DenseNet	0.7322	0.6514	0.5814	0.5209	0.3714	0.6833	2.2655

TABLE II: Performance Comparison of Individual and Fusion-Based CNN Encoders on the UCM Dataset

CNN	BLEU-1	BLEU-2	BLEU-3	BLEU-4	METEOR	ROUGE-L	CIDEr
ConvNext	0.8369	0.7804	0.7312	0.6853	0.4689	0.8037	3.3990
ResNet	0.8297	0.7705	0.7178	0.6683	0.4506	0.7903	3.3329
ResNet	0.8179	0.7607	0.7118	0.6658	0.4583	0.7736	3.3165
DenseNet	0.8222	0.7648	0.7211	0.6714	0.4674	0.7833	3.3419
ConvNext-ResNet	0.8457	0.7919	0.7533	0.7166	0.4833	0.8163	3.4255
ConvNext-ResNet	0.8406	0.7796	0.7289	0.6813	0.4656	0.7996	3.4132
ConvNext-DenseNet	0.8416	0.7834	0.7319	0.6877	0.4798	0.8101	3.4522
ResNet-ResNet	0.8334	0.7739	0.7236	0.6723	0.4580	0.7944	3.4108
ResNet-DenseNet	0.8311	0.7825	0.7230	0.6711	0.4596	0.7998	3.3712
ResNext-DenseNet	0.8367	0.7898	0.7292	0.6736	0.4674	0.8112	3.3919

TABLE III: Performance Comparison of Individual and Fusion-Based CNN Encoders on the RSICD Dataset

CNN	BLEU-1	BLEU-2	BLEU-3	BLEU-4	METEOR	ROUGE-L	CIDEr
ConvNext	0.6327	0.4636	0.3602	0.2903	0.2487	0.4648	0.8272
ResNet	0.6322	0.4621	0.3557	0.2835	0.2489	0.4649	0.8206
ResNet	0.6246	0.4525	0.3463	0.2639	0.2294	0.4448	0.8117
DenseNet	0.6298	0.4566	0.3504	0.2668	0.2207	0.4519	0.8167
ConvNext-ResNet	0.6452	0.4767	0.3732	0.3087	0.2609	0.4827	0.8594
ConvNext-ResNet	0.6414	0.4717	0.3676	0.2970	0.2551	0.4741	0.8429
ConvNext-DenseNet	0.6392	0.4634	0.3609	0.3001	0.2588	0.4744	0.8392
ResNet-ResNet	0.6427	0.4734	0.3684	0.2974	0.2558	0.4743	0.8431
ResNet-DenseNet	0.6345	0.4578	0.3542	0.2741	0.2443	0.4694	0.8346
ResNext-DenseNet	0.6282	0.4552	0.3519	0.2712	0.2311	0.4560	0.8213

temporal dependencies. The outputs from L_1 and G are concatenated and passed through two additional linear layers (L_2 and L_3), with L_3 serving as a softmax layer to generate word probabilities.

A. Fusion of Different Encoders

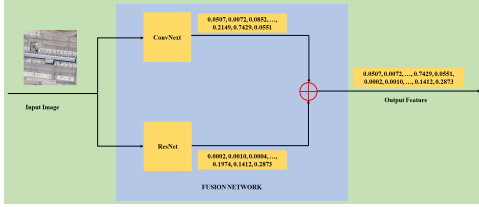


Fig. 2: Architecture of the Fusion Technique Used in Our Model

The proposed method integrates features extracted from two widely used CNN architectures. The fusion strategy is illustrated in Figure 2. Given the vast number of CNN models available, an exhaustive comparison of all individual models and their pairwise combinations is impractical. Therefore, this study focuses on four prominent architectures: ConvNext [2], ResNet [1], ResNext [12], and DenseNet [13]. These models have demonstrated strong feature extraction capabilities in RSIC [4], [14].

As shown in Tables I to III, the combination of features from two different CNNs improves performance compared to the use of a single CNN. This fusion does not add significant computational cost, as CNNs are used solely for feature extraction and remain frozen during training. Since the encoder parameters are not updated, the training remains efficient while benefiting from the diverse spatial and semantic information captured by multiple CNNs. Among the combinations, ConvNext and ResNet yield the best results due to their complementary properties. ConvNext effectively captures global spatial patterns, while ResNet retains fine-grained details through residual connections. Previous studies [4], [14] also highlight their superiority in RSIC tasks. Their fusion results in richer and more robust feature representations, making ConvNext and ResNet the chosen pair for all subsequent experiments in this study.

B. Stacking of Multiple Decoders

Our model uses the Gated Recurrent Unit (GRU) [15] as the decoder. The GRU effectively manages the flow of information through its gating mechanisms, allowing it to maintain crucial temporal dependencies while minimizing computational complexity. Conventional encoder-decoder

architectures typically rely on a single decoder to generate captions in a sequence-to-sequence manner [16], [7], [6], [4]. However, recent work has shown that stacking multiple decoders enhances contextual modeling and hierarchical learning by refining intermediate representations and improving long-term dependency capture [17], [18], [19]. In our approach, we employ a stacked GRU structure in the decoder to enhance the model's ability to process sequential data and to improve its robustness in RSIC. However, simply stacking GRUs sequentially and relying solely on the final layer's output does not always yield the optimal result because deeper networks can suffer from vanishing-gradient problems [20], [21], and important intermediate features might be lost if only the last GRU's output is considered. Furthermore, the information flow between stacking layers may not be efficiently balanced, leading to suboptimal learning. To address these challenges, we explore four different stacking strategies.

1) *Simple Stacking*: The traditional stacking approach, called Simple Stacking (SS), directly utilizes the output of the final decoder layer as the final output of the system. The overall output of the SS system is given below.

$$O = D_n \quad (1)$$

2) *Concatenation-based Stacking*: In Concatenation-based Stacking (CS), the outputs of all decoder layers are concatenated to form the final output, thus preserving a richer set of feature representations. Then, the overall output O of the CS system is given below.

$$O = D_1 | D_2 | \dots | D_n \quad (2)$$

3) *Global Weighted-based Stacking*: In Global Weighted-based Stacking (GWS), a weighted average of the output of all decoder layers is calculated using a single global weight, ensuring a balanced contribution from each layer. The output of the GWS system is given below.

$$O = \sum_{i=1}^n \alpha_i D_i \quad (3)$$

4) *Local Weighted-based Stacking*: In Local Weighted-based Stacking (LWS), a weighted average of the decoder output is calculated using element-specific weights, allowing for finer control over the contribution of each feature to the final output. The output of the LWS system is given below.

$$O = \sum_{i=1}^n W_i \odot D_i \quad (4)$$

Here, n denotes the number of decoders, and D_i represents the output of the i^{th} decoder, while O is the final output of the stacked system. The symbol $|$ indicates the

TABLE IV: Stacked Decoder Results on SYDNEY Dataset

DC	Stack	BLEU-1	BLEU-2	BLEU-3	BLEU-4	METEOR	ROUGE-L	CIDEr
1	NS	0.7679	0.6814	0.6084	0.5458	0.3801	0.7263	2.4515
	SS	0.7576	0.5825	0.5217	0.5672	0.3093	0.7097	2.4382
	CS	0.7784	0.7012	0.6400	0.5853	0.4287	0.7319	2.5614
	GWS	0.7856	0.7106	0.6482	0.5923	0.4195	0.7286	2.5691
	LWS	0.8096	0.7397	0.6580	0.6114	0.4369	0.7461	2.6127
2	NS	0.7535	0.5775	0.5138	0.5587	0.3022	0.7042	2.3934
	SS	0.7539	0.5775	0.5138	0.5587	0.3022	0.7042	2.3934
	CS	0.7680	0.6901	0.6247	0.5654	0.4088	0.7139	2.4645
	GWS	0.8049	0.7319	0.6696	0.6198	0.4348	0.7479	2.6658
	LWS	0.8349	0.7589	0.6952	0.6369	0.4554	0.7767	2.9230
3	NS	0.7357	0.5473	0.5797	0.5186	0.3971	0.6974	2.2434
	SS	0.7576	0.6758	0.6099	0.5520	0.3993	0.7017	2.3367
	CS	0.7576	0.6758	0.6099	0.5520	0.3993	0.7017	2.3367
	GWS	0.7953	0.7212	0.6640	0.6134	0.4266	0.7403	2.6238
	LWS	0.8144	0.7423	0.6849	0.6338	0.4466	0.7587	2.7044
4	NS	0.7506	0.6618	0.5925	0.5331	0.4058	0.7016	2.2981
	SS	0.7646	0.6769	0.6136	0.5577	0.4039	0.7136	2.4011
	CS	0.7646	0.6769	0.6136	0.5577	0.4039	0.7136	2.4011
	GWS	0.7998	0.7282	0.6668	0.6111	0.4288	0.7429	2.5669
	LWS	0.8276	0.7537	0.6904	0.6306	0.4509	0.7706	2.7253

TABLE V: Stacked Decoder Results on UCM Dataset

DC	Stack	BLEU-1	BLEU-2	BLEU-3	BLEU-4	METEOR	ROUGE-L	CIDEr
1	NS	0.8457	0.7919	0.7533	0.7166	0.4833	0.8163	3.4255
	SS	0.8366	0.7764	0.7247	0.6771	0.4558	0.7904	3.4532
	CS	0.8416	0.7860	0.7379	0.6910	0.4642	0.8038	3.5311
	GWS	0.8572	0.8012	0.7510	0.7028	0.4745	0.8089	3.4716
	LWS	0.8663	0.8157	0.7711	0.7276	0.4948	0.8307	3.5485
2	NS	0.8259	0.7606	0.7050	0.6590	0.4528	0.7835	3.4372
	SS	0.8259	0.7606	0.7050	0.6590	0.4528	0.7835	3.4372
	CS	0.8398	0.7848	0.7356	0.6881	0.4622	0.8019	3.5216
	GWS	0.8678	0.8158	0.7706	0.7266	0.4889	0.8265	3.6196
	LWS	0.8805	0.8305	0.7862	0.7511	0.5014	0.8497	3.6806
3	NS	0.8163	0.7583	0.7096	0.6643	0.4481	0.7842	3.4467
	SS	0.8397	0.7844	0.7374	0.6897	0.4685	0.8072	3.4939
	CS	0.8397	0.7844	0.7374	0.6897	0.4685	0.8072	3.4939
	GWS	0.8612	0.8058	0.7581	0.7116	0.4769	0.8173	3.5104
	LWS	0.8661	0.8090	0.7614	0.7170	0.4849	0.8215	3.5838
4	NS	0.8152	0.7551	0.7044	0.6558	0.4407	0.7742	3.3914
	SS	0.8361	0.7818	0.7376	0.6915	0.4633	0.7958	3.4776
	CS	0.8361	0.7818	0.7376	0.6915	0.4633	0.7958	3.4776
	GWS	0.8468	0.7904	0.7416	0.6952	0.4806	0.8143	3.4959
	LWS	0.8613	0.8054	0.7593	0.7157	0.4896	0.8147	3.6018

TABLE VI: Stacked Decoder Results on RSICD Dataset

DC	Stack	BLEU-1	BLEU-2	BLEU-3	BLEU-4	METEOR	ROUGE-L	CIDEr
1	NS	0.6452	0.4767	0.3732	0.3087	0.2609	0.4827	0.8594
	SS	0.6459	0.4786	0.3731	0.3012	0.2599	0.4775	0.8571
	CS	0.6536	0.4871	0.3846	0.3146	0.2698	0.4888	0.8641
	GWS	0.6586	0.4921	0.3881	0.3166	0.2712	0.4921	0.8822
	LWS	0.6683	0.5007	0.3969	0.3265	0.2836	0.5027	0.8818
2	NS	0.6436	0.4759	0.3716	0.3003	0.2606	0.4782	0.8531
	SS	0.6436	0.4759	0.3716	0.3003	0.2606	0.4782	0.8531
	CS	0.6531	0.4869	0.3818	0.3116	0.2671	0.4894	0.8697
	GWS	0.6614	0.5014	0.3984	0.3314	0.2911	0.5134	0.9196
	LWS	0.6796	0.5124	0.4073	0.3365	0.2944	0.5248	0.9423
3	NS	0.6364	0.4687	0.3652	0.2956	0.2578	0.4727	0.8363
	SS	0.6463	0.4797	0.3757	0.3043	0.2530	0.4698	0.8441
	CS	0.6511	0.4846	0.3806	0.3091	0.2637	0.4846	0.8747
	GWS	0.6596	0.4924	0.3873	0.3165	0.2744	0.4938	0.8823
	LWS	0.6579	0.4683	0.3627	0.2906	0.2566	0.4710	0.8250
4	NS	0.6425	0.4734	0.3726	0.3014	0.2490	0.4636	0.8361
	SS	0.6502	0.4812	0.3745	0.2894	0.2511	0.4511	0.8426
	GWS	0.6502	0.4812	0.3745	0.2894	0.2511	0.4511	0.8426
	LWS	0.6519	0.4843	0.3800	0.3089	0.2692	0.4886	0.8653

concatenation operation. The parameter α_i represents a scalar weight, while W_i is a vector weight of the same size as D_i for each D_i . Furthermore, $0 \leq \alpha_i \leq 1$ with constraint $\sum_{i=1}^n \alpha_i = 1$, and $0 \leq W_i^j \leq 1$ with $\sum_{i=1}^n W_i^j = 1$, where W_i^j denotes the value of the characteristic j^{th} of W_i . Both $\alpha = \{\alpha_i \mid i = 1, \dots, n\}$ and $W = \{W_i \mid i = 1, \dots, n\}$ are trainable parameters.

The impact of the depth of the decoder is evaluated in Tables IV to VI, where the number of stacked GRUs (DC) is treated as a hyperparameter ranging from two to five. Configurations beyond five are excluded due to increased computational cost and diminishing returns.

In the SYDNEY and UCM datasets (Tables IV and V), deeper stacks under SS and CS show inconsistent trends, often degrading beyond two layers. SS, in particular, underperforms the single-decoder baseline (NS), probably due to vanishing gradients and limited training data [22]. RSICD maintains stable performance up to three layers, with declines beyond that point, indicating sensitivity to the depth of the decoder.

From the results, we observe that among the stacking strategies, SS and CS are less effective. SS eliminates intermediate outputs, while CS introduces redundancy by treating all outputs equally. Weighted strategies offer a better balance: GWS uses global weights but lacks temporal flexibility, whereas LWS applies adaptive element-wise weights, enabling finer control over temporal dependencies. LWS consistently achieves the best results, with three stacked decoders yielding optimal performance across all datasets.

III. EXPERIMENTAL SETUP

We use a conventional encoder-decoder architecture. Each GRU on the decoder stack (G) has an output size of 256. Linear layers $L1$, $L2$, and $L3$ have output sizes of 256, 512, and one more than the vocabulary size, respectively. GELU is used as the activation function for $L1$ and $L2$, while $L3$ uses *SoftMax*. A dropout rate of 0.5 is applied before $L1$, after the embedding layer (E), before the sequence loss layer (SL), and between consecutive GRUs to prevent overfitting. The embedding size is set to 256.

Training is carried out with a batch size of 64 using the Adam optimizer (learning rate 10^{-4}) and categorical cross entropy as a loss function. An early stopping criterion with a patience of eight epochs is used, monitoring ROUGE-L on the validation set. For caption generation, we apply the comparison-based beam search [3], [7] with a beam width of five, using four similar images. The comparison score is

calculated as the arithmetic mean of BLEU-2, METEOR, and ROUGE-L.

The experiments were carried out using TensorFlow within a Docker environment with GPU support, on a host machine equipped with a *NVIDIA RTX A6000* GPU with 50GB memory and 132GB RAM. During manuscript preparation, ChatGPT and Grammarly were used solely for rephrasing and language refinement, without generating any original technical content.

A. Datasets Used

The performance of the model was evaluated using three widely recognized RSIC datasets: SYDNEY [16], UCM [16], and RSICD [22]. The details of these datasets are provided in the supplementary material. In this study, we used the corrected versions of these datasets [3], which address common issues such as spelling mistakes, grammatical errors, and inconsistent dialect variations of English. We used the same train-validation-test split as defined in these datasets.

B. Performance metrics

The evaluation metrics used in our model include BLEU [23], METEOR [24], ROUGE [25], and CIDEr [26], which are widely adopted in RSIC tasks [16], [22], [3], [4]. More details are provided in the supplementary material.

IV. RESULTS

This section presents a comprehensive evaluation of the proposed model through ablation studies, quantitative comparisons with baseline methods, and visual analysis. The goal is to assess the individual and combined contributions of encoder fusion, decoder stacking, and caption selection strategy.

A. Ablation Studies

To evaluate the contribution of individual components, we compare four encoder-decoder configurations: single encoder with single decoder, fusion-based encoder with single decoder, single encoder with LWS decoder and the proposed fusion-based encoder with LWS decoder.

The results, shown in Tables VII to IX, follow the naming convention where C denotes ConvNext, R denotes ResNet, and FE indicates their fusion. For decoders, NS refers to a single decoder and LWS to Local Weighted-based Stacking with three GRUs (see Section II-B).

TABLE VII: Performance Comparison of Model Variants Through Ablation Studies on SYDNEY Dataset

METHOD	BLEU-1	BLEU-2	BLEU-3	BLEU-4	METEOR	ROUGE-L	CIDEr
C-NS	0.7531	0.6645	0.5982	0.5376	0.3750	0.6951	2.3954
R-NS	0.7363	0.6502	0.5785	0.5138	0.3621	0.6809	2.2526
FE-NS	0.7679	0.6814	0.6084	0.5458	0.3801	0.7263	2.4515
C-LWS	0.8141	0.7321	0.6610	0.6054	0.4369	0.7584	2.7472
R-LWS	0.8056	0.7211	0.6527	0.5924	0.4216	0.7364	2.5743
FE-LWS	0.8349	0.7589	0.6952	0.6369	0.4554	0.7767	2.9230

TABLE VIII: Performance Comparison of Model Variants Through Ablation Studies on UCM dataset

METHOD	BLEU-1	BLEU-2	BLEU-3	BLEU-4	METEOR	ROUGE-L	CIDEr
C-NS	0.8369	0.7804	0.7312	0.6853	0.4689	0.8037	3.3990
R-NS	0.8297	0.7705	0.7178	0.6683	0.4506	0.7903	3.3329
FE-NS	0.8457	0.7919	0.7533	0.7166	0.4833	0.8163	3.4255
C-LWS	0.8655	0.8121	0.7644	0.7192	0.5086	0.8367	3.4958
R-LWS	0.8614	0.8034	0.7526	0.7049	0.4910	0.8194	3.4621
FE-LWS	0.8805	0.8305	0.7862	0.7511	0.5014	0.8497	3.6806

TABLE IX: Performance Comparison of Model Variants Through Ablation Studies on RSICD dataset

METHOD	BLEU-1	BLEU-2	BLEU-3	BLEU-4	METEOR	ROUGE-L	CIDEr
C-NS	0.6327	0.4636	0.3602	0.2903	0.2487	0.4648	0.8272
R-NS	0.6322	0.4621	0.3557	0.2835	0.2489	0.4649	0.8206
FE-NS	0.6452	0.4767	0.3732	0.3087	0.2609	0.4827	0.8594
C-LWS	0.6671	0.5008	0.3996	0.3302	0.2843	0.5066	0.8954
R-LWS	0.6645	0.4981	0.3963	0.3257	0.2849	0.5010	0.8684
FE-LWS	0.6796	0.5124	0.4073	0.3365	0.2944	0.5248	0.9423

TABLE X: Experimental Results of Baseline Methods and Different Searching Techniques on SYDNEY Dataset

METHOD	BLEU-1	BLEU-2	BLEU-3	BLEU-4	METEOR	ROUGE-L	CIDEr
R-BOW [22]	0.5310	0.4076	0.3319	0.2788	0.2490	0.4922	0.7019
L-FV [22]	0.6331	0.5332	0.4735	0.4303	0.2967	0.5794	1.4760
CSMLF [27]	0.4441	0.3369	0.2815	0.2408	0.1576	0.4018	0.9378
CSMLF-FT [27]	0.5998	0.4583	0.3869	0.3433	0.2475	0.5018	0.7555
SVM-DBOW [6]	0.7787	0.6835	0.6023	0.5305	0.3797	0.6992	2.2722
SVM-DCONC [6]	0.7547	0.6711	0.5970	0.5308	0.3643	0.6746	2.2222
TrTr-CMR [28]	0.8270	0.6994	0.6002	0.5199	0.3803	0.7220	2.2728
TextGCN [3]	0.7680	0.6892	0.6261	0.5786	0.4009	0.7314	2.8595
FE-LWS	0.8349	0.7589	0.6952	0.6369	0.4554	0.7767	2.9230

TABLE XI: Experimental Results of Baseline Methods and Different Searching Techniques on UCM Dataset

METHOD	BLEU-1	BLEU-2	BLEU-3	BLEU-4	METEOR	ROUGE-L	CIDEr
R-BOW [22]	0.4107	0.2249	0.1452	0.1095	0.1098	0.3439	0.3071
L-FV [22]	0.5897	0.4668	0.4080	0.3683	0.2698	0.5595	1.8438
CSMLF [27]	0.3874	0.2145	0.1253	0.0915	0.0954	0.3599	0.3703
CSMLF-FT [27]	0.3671	0.1485	0.0763	0.0505	0.0944	0.2986	0.1351
SVM-DBOW [6]	0.7635	0.6664	0.5869	0.5195	0.3654	0.6801	2.7142
SVM-DCONC [6]	0.7653	0.6947	0.6417	0.5942	0.3702	0.6877	2.9228
TrTr-CMR [28]	0.8156	0.7091	0.6220	0.5469	0.3978	0.7442	2.4742
TextGCN [3]	0.8461	0.7844	0.7386	0.6930	0.4868	0.8071	3.4077
FE-LWS	0.8805	0.8305	0.7862	0.7511	0.5014	0.8497	3.6806

TABLE XII: Experimental Results of Baseline Methods and Different Searching Techniques on RSICD Dataset

METHOD	BLEU-1	BLEU-2	BLEU-3	BLEU-4	METEOR	ROUGE-L	CIDEr
R-BOW [22]	0.4401	0.2383	0.1514	0.1041	0.1684	0.3605	0.4667
L-FV [22]	0.4342	0.2453	0.1634	0.1175	0.1712	0.3818	0.6531
CSMLF [27]	0.3759	0.3859	0.2832	0.2217	0.2128	0.4455	0.5297
CSMLF-FT [27]	0.5106	0.2911	0.1903	0.1352	0.1693	0.3789	0.3388
SVM-DBOW [6]	0.6112	0.4277	0.3153	0.2411	0.2303	0.4588	0.6825
SVM-DCONC [6]	0.5999	0.4347	0.3355	0.2689	0.2299	0.4577	0.6854
TrTr-CMR [28]	0.6201	0.3937	0.2671	0.1932	0.2399	0.4865	0.7518
TextGCN [3]	0.6513	0.4819	0.3747	0.3085	0.2752	0.4804	0.8266
FE-LWS	0.6796	0.5124	0.4073	0.3365	0.2944	0.5248	0.9423

The results indicate that both encoder fusion and decoder stacking improve performance, with the FE-LWS configuration achieving the highest scores across all datasets. In particular, LWS offers greater performance gains than encoder fusion alone, highlighting its effectiveness even when used with a single CNN.

B. Numerical Evaluation

Tables X to XII compares various baseline methods. R-BOW and L-FV [22] use handcrafted sentence representations with RNN and LSTM decoders, respectively. CSMLF and its fine-tuned variant [27] extend this for multi-sentence captioning. SVM-DBOW and SVM-DCONC [6] apply SVMs with bag-of-words and concatenated sentence features. TrTr-CMR [28] combines a Swin Transformer encoder with a cross-modal transformer decoder. TextGCN [3] aligns the embeddings of the decoder with frozen TextGCN output. Our model, FE-LWS, combines dual CNN encoders with stacked GRUs and local weighted aggregation to enhance semantic representation. This method improves performance by effectively integrating the encoding and decoding strategies. The results demonstrate that the proposed FE-LWS model achieves substantially superior performance compared to the baseline methods.

The qualitative evaluation is provided in the supplementary material, where the captions are evaluated by a human annotator¹.

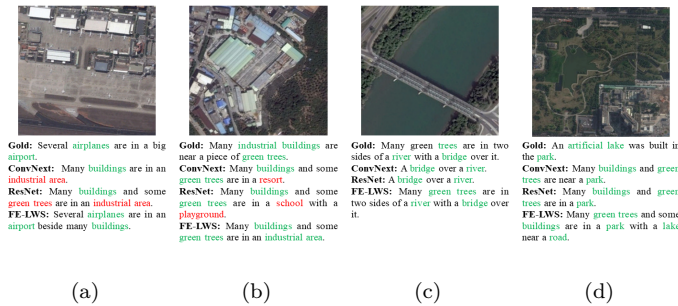


Fig. 3: Examples of RS Image Captioning by Different Methods

¹The annotator has several years of experience in RSIC.

C. Visual Interpretation

We present qualitative results from the test sets of three datasets in Figure 3, comparing the proposed model (FE-LWS) with ground-truth captions (Gold) and conventional encoder-decoder models (ConvNext and ResNet). In the first two examples (Figures 3a and 3b), the proposed model correctly classifies the images, while ConvNext and ResNet fail. In Figure 3a, ConvNext and ResNet misclassify the image as *industrial area*, whereas the proposed model accurately identifies it. In Figure 3b, ConvNext misclassifies the image as *resort* and ResNet as *school*, while the proposed model generates a meaningful and accurate caption. In the next two examples (Figures 3c and 3d), the proposed model enhances the quality of the captions by incorporating more detailed information. In Figure 3c, all models detect *bridge* and *river*, while the proposed model also captures *trees*. In Figure 3d, while all models detect *park*, the proposed model further identifies *lake* and *road*.

V. CONCLUSION

Existing RSIC methods focus primarily on decoder enhancements, while giving limited attention to optimizing feature extraction during encoding. Moreover, most approaches rely on a single encoder and decoder, which restricts the model's ability to handle the complex spatial and semantic characteristics of remote sensing images. To address these limitations, we propose a framework that combines features from two complementary CNN encoders and employs a stacked GRU-based decoder with a locally weighted aggregation strategy. This combination enables a more effective integration of multilevel semantic information, resulting in captions that are contextually rich and semantically accurate. The experimental results across multiple datasets demonstrate the superior performance of the proposed method compared to existing baselines. Fusion-based encoding improves spatial detail extraction, while weighted decoder stacking improves semantic coherence. Although the model shows robust performance, challenges may still arise when dealing with previously unseen or underrepresented image classes. Future research will explore directions to further enhance the generalization and robustness of the model without compromising efficiency. These advances are expected to improve the adaptability and reliability of RSIC in broader applications.

VI. DATASETS USED

The specifications of the three datasets used in our model are outlined below.

- **SYDNEY:** SYDNEY [16] dataset consists of 613 images, with 497 allocated for training, 58 for testing, and 58 for validation. It is derived from the Sydney dataset [29] and has been carefully curated to include seven distinct categories: *airport*, *industrial*, *meadow*, *ocean*, *residential*, *river*, and *runway*, through thoughtful cropping and selection.
- **UCM:** UCM [16] dataset consists of 2,100 images, with 1,680 allocated for training, 210 for testing, and 210 for validation. It is derived from the *UC Merced Land Use* dataset [30], which features 21 land use image classes, each containing 100 images. These classes include *agriculture*, *airport*, *baseball diamond*, *beach*, *buildings*, *chaparral*, *denseresidential*, *forest*, *freeway*, *golfcourse*, *harbour*, *intersection*, *mediumresidential*, *mobilehome*, *overpass*, *parking*, *river*, *runway*, *sparseresidential*, *storage tanks* and *tennis court*.
- **RSICD:** RSICD [22] dataset includes a substantial collection of 10921 images, with 8034 designated for training, 1093 for testing and 1094 for validation. Sourced from a variety of platforms such as Google Earth [31], Baidu Map, MapABC, and Tianditu, this dataset encompasses 31 distinct image classes, including *airport*, *bareland*, *baseballfield*, *beach*, *bridge*, *center*, *church*, *commercial*, *denseresidential*, *desert*, *farmland*, *forest*, *industrial*, *meadow*, *mediumresidential*, *mountain*, *park*, *parking*, *playground*, *pond*, *port*, *railwaystation*, *resort*, *river*, *school*, *sparseresidential*, *square*, *stadium*, *storage tanks*, and *viaduct*.

VII. PERFORMANCE METRICS

The evaluation metrics used to assess our model's performance are described below.

- **BLEU:** Bilingual Evaluation Understudy [23] measures n-gram overlap between generated and reference captions. Calculate the geometric mean of the precision of n grams (BLEU-1 to BLEU-4) and apply a brevity penalty to discourage short outputs.
- **METEOR:** Metric for Evaluation of Translation with Explicit Ordering [24] incorporates stemming, synonymy, and word order. It balances precision and recall with an emphasis on alignment and content accuracy.
- **ROUGE:** Recall-Oriented Understudy for Gisting Evaluation [25] is a recall-based metric that measures n-gram overlap. We use ROUGE-L, which focuses on the longest common subsequence (LCS).
- **CIDEr:** Consensus-based Image Description Evaluation [26] evaluates the similarity between generated and human-written captions by measuring consensus across multiple references, highlighting the relevance and agreement of the content.

VIII. SUBJECTIVE EVALUATION

TABLE XIII: Subjective Evaluation of Different CNNs on Three Datasets (in %)

Method	SYDNEY			UCM			RSICD		
	R	W	U	R	W	U	R	W	U
ConvNext	89.66	1.72	8.62	89.04	4.29	6.67	82.25	5.31	12.44
ResNet	87.93	3.45	8.62	88.09	5.24	6.67	81.43	5.03	13.54
FE-LWS	94.83	3.45	1.72	92.86	5.24	1.90	83.72	6.95	9.33

Unlike classification, multiple captions can describe the same image with similar effectiveness. Hence, relying solely on the test captions (five for all three data sets) to evaluate the predicted captions is not justified [22], [4]. For this reason, we performed a subjective evaluation. In this process, we assigned a human annotator with expertise in this field to assess the quality of the captions generated. This evaluation provides insights into caption quality from the perspective of human psychology. In our work, we used three labels to assess the quality of the generated captions, as discussed below.

- **Related:** The generated caption accurately describes the input image.
- **Partially Related:** The generated caption describes the input image but contains major errors or flaws.
- **Unrelated:** The generated caption is completely incorrect and does not describe the input image in any meaningful way.

Table XIII presents the subjective evaluation results, comparing our model (FE-LWS) with conventional encoder-decoder models, where ConvNext and ResNet are used as encoders, respectively. The results indicate that our model outperforms other models.

REFERENCES

- [1] K. He, X. Zhang, S. Ren, and J. Sun, "Deep residual learning for image recognition," in *Proceedings of the IEEE conference on computer vision and pattern recognition*, 2016, pp. 770–778.
- [2] Z. Liu, H. Mao, C.-Y. Wu, C. Feichtenhofer, T. Darrell, and S. Xie, "A convnet for the 2020s," in *Proceedings of the IEEE/CVF conference on computer vision and pattern recognition*, 2022, pp. 11 976–11 986.
- [3] S. Das and R. Sharma, "A textgcn-based decoding approach for improving remote sensing image captioning," *IEEE Geoscience and Remote Sensing Letters*, 2024.
- [4] S. Das, A. Khandelwal, and R. Sharma, "Unveiling the power of convolutional neural networks: A comprehensive study on remote sensing image captioning and encoder selection," in *2024 International Joint Conference on Neural Networks (IJCNN)*. IEEE, 2024, pp. 1–8.
- [5] M. Tanti, A. Gatt, and K. P. Camilleri, "Where to put the image in an image caption generator," *Natural Language Engineering*, vol. 24, no. 3, pp. 467–489, 2018.
- [6] G. Hoxha and F. Melgani, "A novel svm-based decoder for remote sensing image captioning," *IEEE Transactions on Geoscience and Remote Sensing*, vol. 60, pp. 1–14, 2021.
- [7] G. Hoxha, F. Melgani, and J. Slaghenauuffi, "A new cnn-rnn framework for remote sensing image captioning," in *2020 Mediterranean and Middle-East Geoscience and Remote Sensing Symposium (M2GARSS)*. IEEE, 2020, pp. 1–4.
- [8] X. Li, A. Yuan, and X. Lu, "Multi-modal gated recurrent units for image description," *Multimedia Tools and Applications*, vol. 77, no. 22, pp. 29 847–29 869, 2018.
- [9] O. Vinyals, A. Toshev, S. Bengio, and D. Erhan, "Show and tell: A neural image caption generator," in *Proceedings of the IEEE conference on computer vision and pattern recognition*, 2015, pp. 3156–3164.

- [10] E. Alabdulkreem, N. Alruwais, H. Mahgoub, A. K. Dutta, M. Khalid, R. Marzouk, A. Motwakel, and S. Drar, "Sustainable groundwater management using stacked lstm with deep neural network," *Urban Climate*, vol. 49, p. 101469, 2023.
- [11] V. Vakharia, M. Shah, P. Nair, H. Borade, P. Sahlot, and V. Wankhede, "Estimation of lithium-ion battery discharge capacity by integrating optimized explainable-ai and stacked lstm model," *Batteries*, vol. 9, no. 2, p. 125, 2023.
- [12] S. Xie, R. Girshick, P. Dollár, Z. Tu, and K. He, "Aggregated residual transformations for deep neural networks," in *Proceedings of the IEEE conference on computer vision and pattern recognition*, 2017, pp. 1492–1500.
- [13] G. Huang, Z. Liu, L. Van Der Maaten, and K. Q. Weinberger, "Densely connected convolutional networks," in *Proceedings of the IEEE conference on computer vision and pattern recognition*, 2017, pp. 4700–4708.
- [14] S. Das, S. Gupta, K. Kumar, and R. Sharma, "Good representation, better explanation: Role of convolutional neural networks in transformer-based remote sensing image captioning," *arXiv preprint arXiv:2502.16095*, 2025.
- [15] R. Khan, M. S. Islam, K. Kanwal, M. Iqbal, M. I. Hossain, and Z. Ye, "A deep neural framework for image caption generation using gru-based attention mechanism," *arXiv preprint arXiv:2203.01594*, 2022.
- [16] B. Qu, X. Li, D. Tao, and X. Lu, "Deep semantic understanding of high resolution remote sensing image," in *2016 International conference on computer, information and telecommunication systems (Cits)*. IEEE, 2016, pp. 1–5.
- [17] M. A. Alghamdi, S. Abdullah, and M. Ragab, "Predicting energy consumption using stacked lstm snapshot ensemble," *Big Data Mining and Analytics*, vol. 7, no. 2, pp. 247–270, 2024.
- [18] X. Liang, C. Li, and L. Tian, "Clustering-based mask recovery for image captioning," *Neurocomputing*, vol. 599, p. 128127, 2024.
- [19] Y. Ren, R. Zhang, and F. Gao, "A network structure for industrial process fault diagnosis based on hyper feature extraction and stacked lstm," *Chemical Engineering Science*, vol. 287, p. 119745, 2024.
- [20] J. Gu, J. Cai, G. Wang, and T. Chen, "Stack-captioning: Coarse-to-fine learning for image captioning," in *Proceedings of the AAAI conference on artificial intelligence*, vol. 32, no. 1, 2018.
- [21] M. O. Turkoglu, S. D'Aronco, J. D. Wegner, and K. Schindler, "Gating revisited: Deep multi-layer rnns that can be trained," *IEEE Transactions on Pattern Analysis and Machine Intelligence*, vol. 44, no. 8, pp. 4081–4092, 2021.
- [22] X. Lu, B. Wang, X. Zheng, and X. Li, "Exploring models and data for remote sensing image caption generation," *IEEE Transactions on Geoscience and Remote Sensing*, vol. 56, no. 4, pp. 2183–2195, 2017.
- [23] K. Papineni, S. Roukos, T. Ward, and W.-J. Zhu, "Bleu: a method for automatic evaluation of machine translation," in *Proceedings of the 40th Annual Meeting of the Association for Computational Linguistics*. Philadelphia, Pennsylvania, USA: Association for Computational Linguistics, Jul. 2002, pp. 311–318. [Online]. Available: <https://aclanthology.org/P02-1040>
- [24] A. Lavie and A. Agarwal, "METEOR: An automatic metric for MT evaluation with high levels of correlation with human judgments," in *Proceedings of the Second Workshop on Statistical Machine Translation*. Prague, Czech Republic: Association for Computational Linguistics, Jun. 2007, pp. 228–231. [Online]. Available: <https://aclanthology.org/W07-0734>
- [25] C.-Y. Lin, "ROUGE: A package for automatic evaluation of summaries," in *Text Summarization Branches Out*. Barcelona, Spain: Association for Computational Linguistics, Jul. 2004, pp. 74–81. [Online]. Available: <https://aclanthology.org/W04-1013>
- [26] R. Vedantam, C. Lawrence Zitnick, and D. Parikh, "Cider: Consensus-based image description evaluation," in *Proceedings of the IEEE conference on computer vision and pattern recognition*, 2015, pp. 4566–4575.
- [27] B. Wang, X. Lu, X. Zheng, and X. Li, "Semantic descriptions of high-resolution remote sensing images," *IEEE Geoscience and Remote Sensing Letters*, vol. 16, no. 8, pp. 1274–1278, 2019.
- [28] Y. Wu, L. Li, L. Jiao, F. Liu, X. Liu, and S. Yang, "Trtr-cmr: Cross-modal reasoning dual transformer for remote sensing image captioning," *IEEE Transactions on Geoscience and Remote Sensing*, 2024.
- [29] F. Zhang, B. Du, and L. Zhang, "Saliency-guided unsupervised feature learning for scene classification," *IEEE Transactions on Geoscience and Remote Sensing*, vol. 53, no. 4, pp. 2175–2184, 2014.
- [30] Y. Yang and S. Newsam, "Bag-of-visual-words and spatial extensions for land-use classification," in *Proceedings of the 18th SIGSPATIAL international conference on advances in geographic information systems*, 2010, pp. 270–279.
- [31] G.-S. Xia, J. Hu, F. Hu, B. Shi, X. Bai, Y. Zhong, L. Zhang, and X. Lu, "Aid: A benchmark data set for performance evaluation of aerial scene classification," *IEEE Transactions on Geoscience and Remote Sensing*, vol. 55, no. 7, pp. 3965–3981, 2017.